Journal of Marine Research, 51, 293–322, 1993

Buoyancy and wind forcing of a coastal current

by Andreas Münchow[1,2] and Richard W. Garvine[1]

ABSTRACT

Local winds and lateral buoyancy fluxes from estuaries constitute two major forcing mechanisms on the inner continental shelf of the Mid Atlantic Bight on the eastern seaboard of the U.S.A. We report observations of the resulting coastal current that suggest a linear superposition of the wind and buoyancy forced motions. This current, which we term the Delaware Coastal Current, has a mean flow of about 10 cm/s in the direction of Kelvin wave phase propagation. It opposes the generally upwelling favorable local winds there. The same winds, however, force important across-shelf flows that agree qualitatively with Ekman dynamics with Ekman numbers that are O(1). Velocity fluctuations at current meter mooring are consistent with the above dynamics, and explain the local hydrography well. Trajectories from drifters and derived velocity fields, too, reveal consistent flow patterns. We further find that Lagrangian and Eulerian integral time scales are similar, implying a linear flow field. We estimate dispersion coefficients for this buoyancy driven coastal current to be about 2000 and 200 m^2/s in the along- and across-shelf direction, respectively. Our results disagree both qualitatively and quantitatively with those of a recent numerical model of the study area.

1. Introduction

Local winds and buoyancy fluxes often dominate the dynamics of inner continental shelves. Tangential stresses applied to the sea surface by the local winds transfer momentum from the atmosphere to the coastal ocean. Lateral buoyancy fluxes from estuaries to the shelf produce pressure gradients that often are balanced by the Coriolis force of an along-shore current. While the wind forced motion on continental shelves has been examined extensively over the last decades, see reviews of Allen *et al.* (1983), Winant (1980), and Brink (1991), the buoyancy forced motion has only recently been studied. Major buoyancy driven current systems in deeper waters are reported along the coasts of Alaska (Royer, 1983), Norway (Johannesen *et al.,* 1989), and western Australia (Griffiths and Pearce, 1985). These currents generally detach from the bottom and thus contrast with the buoyancy driven flow that we study here in water as shallow as one Ekman layer depth. Such shallow water flows are common and often result from estuarine outflows. Van der Giessen (1990) describes how the

1. College of Marine Studies, University of Delaware, Newark, Delaware, 19716, U.S.A.
2. Present address: Center for Coastal Studies, Scripps Institution of Oceanography, La Jolla, California, 92093-0209, U.S.A.

Rhine outflow affects the entire Dutch coastal zone. Münchow and Garvine (1992) and Wong and Münchow (1992) report observations of the Delaware Coastal Current as far as 80 km from its buoyancy source, the mouth of the Delaware Estuary. Blanton (1981) invokes thermal wind and Ekman dynamics to explain coastal flows off Georgia, while Bowman and Iverson (1978) present preliminary evidence of a coastal current that originates from the Hudson River outflow. Simpson and Hill (1986) introduce the Scottish Coastal Current. Finally, observations from the East China Sea (Beardsley *et al.*, 1985) trace the outflow from the Yangtze River that discharges huge amounts of sediment into the coastal ocean. In all of the above studies Coriolis forces constitute a major term in the across-shelf momentum balance while wind forcing certainly affects the flows. Most studies, however, concentrate either on the buoyancy or the wind driven motion. Possible interactions between the two processes are often ignored. The resolution of both processes simultaneously and their respective importance is indeed difficult, mainly because spatial scales of the wind forced motion often exceed those of the buoyancy forced motion while the reverse holds for temporal scales. Some overlap of scales, however, always occurs.

Near the Delaware Estuary on the eastern seaboard of the U.S.A. we repeatedly surveyed the inner continental shelf where depths are shallower than 30 m. Here a persistent coastal current, the Delaware Coastal Current, forms (Garvine, 1991) downstream of the estuary. Upstream the Hudson Coastal Current appears intermittently. Our observations describe the mixing and the circulation that buoyancy and wind forcing initiate. The shallow water implies that surface and bottom Ekman layers might overlap. Most numerical and analytical models of shelf circulation exclude this region from the model domain. Mitchum and Clarke (1986) are a notable exception, but even their focus is on a new, better coastal boundary condition for vorticity wave models that apply beyond the near shore coastal zone. This domain, however, can extend several internal deformation radii across the shelf, as it does in our application. Pettigrew (1981) and Csanady (1978) first studied this "coastal boundary layer" but they excluded buoyancy forcing and assumed alongshore scales that are much larger than across-shore ones. In our study region buoyancy forcing is as important as wind forcing and both the flow and the density fields vary along the shelf. In a recent paper (Münchow and Garvine, 1992) we focused on the dynamical properties of the Delaware Coastal Current. Here we study the flow and density fields of this current in detail and seek to relate it to the two dominant forcing agents: buoyancy and wind.

We organize our study as follows. In the next section we introduce both our study area and data sources. In Section 3 we describe our observations qualitatively and then, in Section 4, we describe them statistically. We employ both Eulerian and Lagrangian statistics that provide a consistent view of the flow field. Section 5 concludes this study and compares the main results with those of a numerical model of our study area.

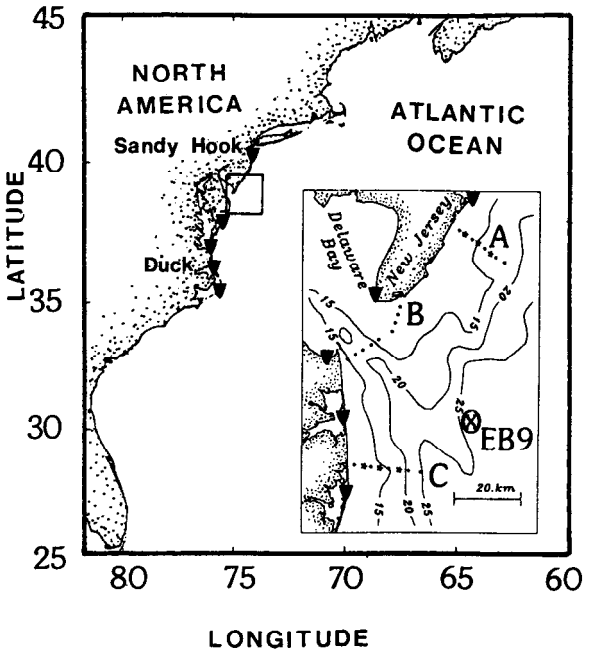

Figure 1. Map of the study area. The insert is an enlargement of the area near 38N and 75W. The triangles mark the location of coastal tide gauges and EB9 represents a meteorological buoy. We denote the three major transects as A, B, and C. Current meter mooring locations we depict as filled stars on transect A and C. The dots on each transect mark the location of CTD and ADCP stations.

2. Study area and data sources

In May and June of 1989 we intensely surveyed the inner continental shelf 100 km in the along- and 30 km in the across-shore direction in an area that centers on the mouth of the Delaware Estuary. Figure 1 shows three major transect lines, the location of 6 current meter moorings, and the bottom topography. We deployed a total of 10 electromagnetic S4 current meters of InterOcean Inc. on transects A and C. The two most inshore mooring locations on each transect contained two current meters, namely one at 6 m and the other at 10 m below the surface. The most offshore mooring contained a single instrument at 6 m depth. The water depths at the three mooring locations of transect A and C were (14, 13, 15) m and (14, 17, 18) m, respectively. The instruments collected averaged temperature and conductivity, and vector averaged velocities from 5 min. records at 2 Hz every 30 min. On transects A, B, and C we also collected velocity data with a 307 kHz vessel mounted acoustic Doppler current profiler (ADCP) of RDI. We omit a description of this instrument here and instead refer to Münchow *et al.* (1992a) for a discussion of its performance, calibration, and use to obtain subtidal currents. At every ADCP station we collected hydrographic data with a Brown Mark IIIb CTD. Vertical profiles of salinity from the

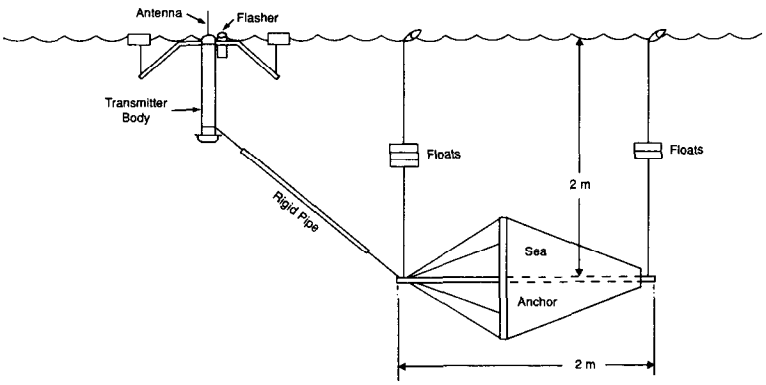

Figure 2. Scale drawing of the drifter design.

latter instrument complement horizontal maps of near surface salinity that we constructed from data which a thermosalinograph provided every 30 s along the ship track.

We also repeatedly deployed, retrieved, and redeployed between 4 and 7 drogued drifters that we tracked with the ARGOS satellite system. We illustrate our drifter in Figure 2. It had two principal parts, a surface element and a drogue. In the surface element we housed an ARGOS transmitter in a water-tight cylindrical body together with a battery. The antenna extended 16 cm above the top cap and above the water surface. Four arms extended from the top cap laterally to the ends of which we fixed floatation that kept the surface element upright. We attached a strobe flasher to the cylindrical body to aid nighttime recovery. A tether line extended from the bottom of the cylinder laterally and downward to the drogue. This line passed through a rigid section of pipe that prevented the drogue assembly from fouling the surface element. The drogue consisted of a commercial sea anchor of 2 m length suspended horizontally from floatation so that its center line was at 2 m depth. Apart from the use of a sea anchor, this design is similar to that of Davis *et al.* (1982). It minimizes spurious drift induced by surface gravity wave rectification and wind drag.

3. Observations

We collected data within the Delaware Coastal Current with moored instruments, drifters, and shipboard profiling systems. In Figure 3 we depict time series of currents 6 m below the surface and those of wind and freshwater discharge rates. To all data we applied a Lanczos low-pass filter that passes 10 and 90% of the signal at 30 and 60 hours, respectively. The freshwater discharge from the Delaware River constitutes the main buoyancy source for the shelf of our study area. It varies at weekly and monthly time scales. In contrast, the local winds change almost daily, but during the study period blew dominantly from the south, and thus caused upwelling favorable conditions. The currents, however, often oppose these winds as a result of strong buoyancy forcing. Münchow and Garvine (1992) stress that buoyant coastal current

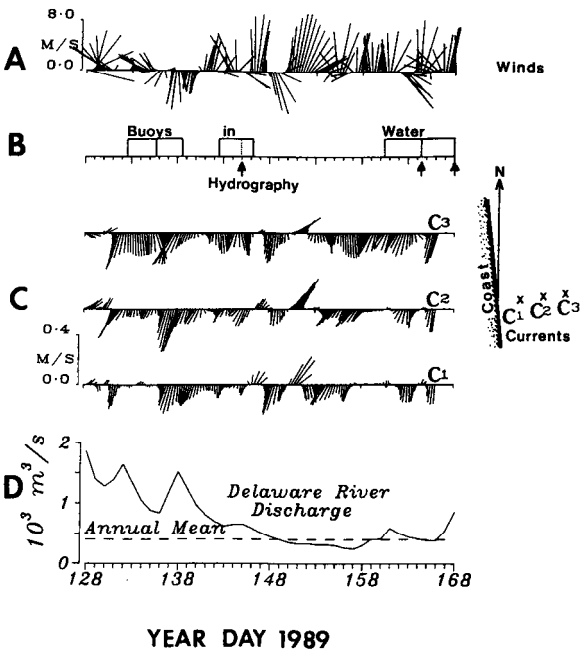

Figure 3. Time series of (a) winds, (b) drifter deployments, (c) currents, and (d) freshwater discharge rates.

waters generally contact the bottom and that a region of large density gradients seaward of our mooring array separates inshore buoyant waters from ambient shelf ones. Hence our current meters at 6 m below the surface are generally well within the coastal current. Strong upwelling favorable wind events, however, occasionally induce vertical stratification which places our 6 m instruments close to the pycnocline. Nevertheless even during a rare flow reversal near day 150 (Fig. 3) associated with such an event, the currents at 6 m have a strong off-shore component (Fig. 3). This response is qualitatively consistent with Ekman dynamics. We thus conclude that our instruments 6 m below the surface are always within the surface Ekman layer. Both the hydrography and the statistical analysis of across-shore currents will reveal this response in more detail. First, however, we quantify the horizontal buoyancy flux from the Delaware Estuary into the coastal ocean before we discuss the inner shelf hydrography proper.

a. Buoyancy fluxes. On two occasions we profiled both the density and the flow field along transects B and C (Fig. 1) with CTD and ADCP instruments for more than a tidal cycle. These data enable us to estimate horizontal buoyancy fluxes b_h as

$$b_h(y,z,t) = \frac{\rho_0 - \rho(y,z,t)}{\rho_0} g\, q_n(y,z,t)$$

where g is the gravitational constant, (y, z, t) are the lateral, vertical and temporal co-ordinates, while ρ and q_n are the density and velocity component normal to the transect, respectively. The reference density ρ_0 we take as that of the ambient shelf water, i.e., $\rho_0 = 1025.5$ kg/m^3. In all the following positive fluxes are seaward from the estuary and downstream, i.e., in the direction of Kelvin wave phase propagation on the shelf. In order to estimate the synoptic distribution of density and velocity within the transect we fitted the following model to the data at each point (y_i, z_j) of the transect, i.e.,

$$\psi(y_i, z_j, t) = \psi_0(y_i, z_j) + \psi_1(y_i, z_j) \cos(\omega t + \theta(y_i, z_j)).$$

Here ψ represents either ρ or q_n and the model parameters ψ_0, ψ_1, and θ are determined by a least square error criterion (Münchow *et al.,* 1992a). The frequency ω represents the semi-diurnal M_2 tidal constituent. Figure 4 demonstrates the fit for a point on transect B at 5 m depth. It compares the prediction ψ with the data. Time, however, we refer to the stage of the M_2 sea level at a nearby coastal tide gauge station, i.e., zero time corresponds to local high water. This representation allows us to overlay the data and predictions from an April experiment with those from one in June of 1989. The modestly different phases during each experiment reflect the impact of a second, unresolved tidal constituent that modulates the velocity and density fluxes at longer time scales. The tidal buoyancy flux, however, is large, typically 0.020 m^2/s^3, and thus masks the subtidal flux. Nevertheless, the latter subtidal flux is the primary cause of the buoyancy driven coastal current on the shelf.

Next we discuss the subtidal signal ψ_0 that (in units of flux per unit area) never exceeds 0.003 m^2/s^3 (Fig. 5). The subtidal fluxes of transect B are positive (seaward) only over the deep channel at the mouth of the estuary (Fig. 5a) while they are small but negative over the remainder of the transect. On the shelf, by contrast, data from transect C (Fig. 5b) give fluxes that are always positive, i.e., downstream. Note, however, that the maximum buoyancy fluxes occur about 12 km from the coast where, as we will show later, we find maximum correlations between along-shelf currents and freshwater discharge rates from the Delaware River.

In order to summarize our buoyancy flux calculations we integrate the flux over each transect and present the results in Table 1. These estimates, as well as those that we presented above, are order of magnitude estimates only. The ADCP does not measure currents near the surface or bottom. The cross-sectional integral of b_h thus misses about 30% of the transect area. We expect, however, to underestimate the buoyancy flux, because the estuary probably exports more buoyancy near the surface than it imports near the bottom. A 10 km wide, 5 m deep layer with a density 1023 kg/m^3 that moves with a speed of 10 cm/s would represent an additional buoyancy flux of 100 m^4/s^3. This uncertainty exceeds the uncertainty due to inaccurate subtidal ADCP velocities. The latter introduce less than 1 cm/s bias in the along-shelf (across-track) direction (Münchow *et al.,* 1992a). The integral of the flux reduces the scatter associated with the ADCP velocity estimation.

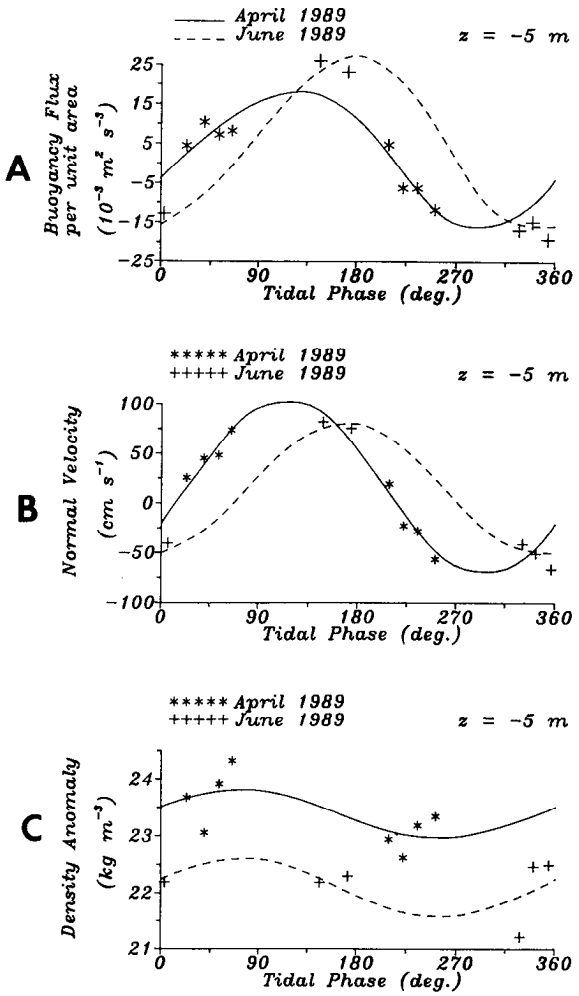

Figure 4. (a) Tidal buoyancy fluxes, (b) flow velocity, and (c) density through an M_2 tidal cycle 5 m below the water surface on transect B over the deep channel. Symbols represent data while the solid and dashed lines indicate the tidal fit for April and June, respectively. Positive currents and fluxes are seaward.

At the upstream transect A weak and negative (upstream) buoyancy fluxes indicate that during our surveys no buoyant water enters our study area from an upstream source. The fluxes at transect A are probably a consequence of upwelling favorable winds. Downstream at transect C, in contrast, strong and positive (downstream) buoyancy fluxes indicate an upstream source: the discharge from the Delaware Estuary. Indeed in April the total fluxes across transects B and C are very similar; however, in June they are not. We here explain both the agreement in April and the disagreement in June with the time that elapsed between profiling the two transects. We always profiled the estuarine transect B prior to the shelf transect C.

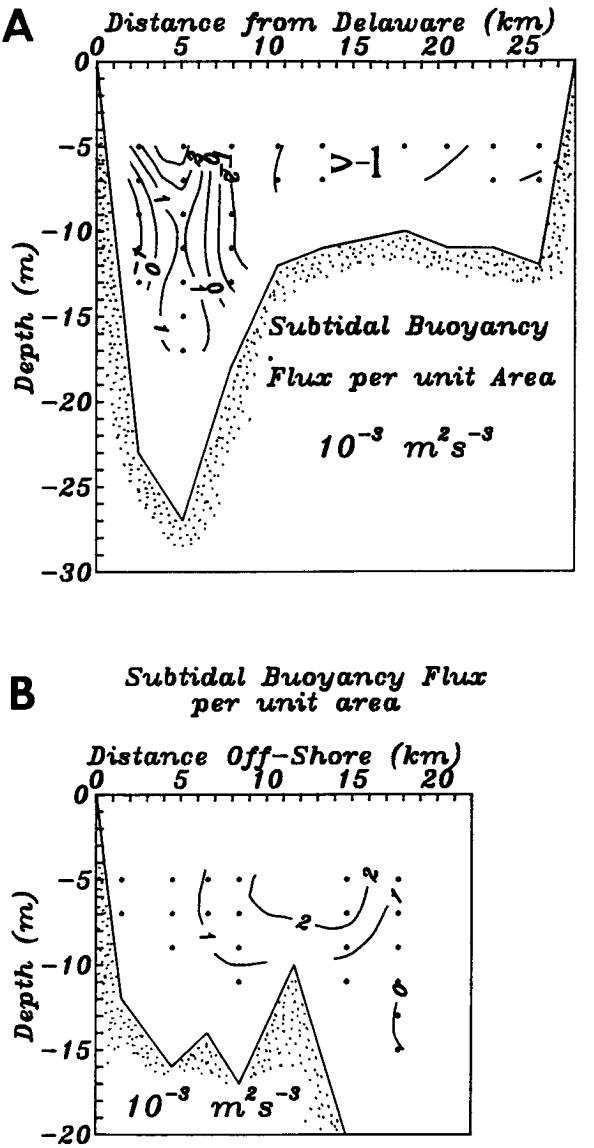

Figure 5. Subtidal horizontal buoyancy fluxes per unit area on (a) transect B at the estuary mouth and (b) transect C downstream in the coastal current for June 1989.

The elapsed time between profiling each transect was 40 and 20 hours in April and June, respectively. A particle that moves with the typical speed of 20 cm/s from transect B needs 45 hours to reach transect C. We thus conclude that in April we observed the same buoyant waters at both locations while in June we did not. We also conclude that buoyancy fluxes on the shelf vary at almost daily time scales, most likely

Table 1. Subtidal buoyancy flux across transects. See Figure 1 for locations. Time Δt refers to the time lag between the profiling of transect B and transect C. Positive fluxes are seaward (downstream). Units are (m^4/s^3).

	Total			Seaward (downstream)			Landward (upstream)			Time (hrs)
Transect	A	B	C	A	B	C	A	B	C	Δt
April	−6	70	60	1	110	70	7	40	10	40
June	−26	−80	160	0	60	160	24	140	0	20
Mean	−16	−5	110	0	85	115	16	90	5	

as a consequence of wind forcing. Winds were light (<1 m/s) in April while they were moderately strong (>5 m/s) in June. Next, however, we discuss the hydrography just prior and during our June experiment in detail. It reveals how buoyancy and wind forcing interact during a strong upwelling favorable event.

b. Hydrography and velocity field. Salinity is an excellent tracer of estuarine waters on the shelf. In our study area density varies almost linearly with salinity. We present three maps of surface salinity from the thermosalingraph in Figures 6 and 7 noting that we completed each survey within 19 (Figs. 6 and 7b) and 23 (Fig. 7a) hours. We augment each map with a vertical salinity transect across the shelf in order to depict the salinity distribution in three dimensions. Figure 6 represents the salinity field in May on day 145 during light but upwelling favorable winds. Near the estuary buoyant waters form a narrow zone with large lateral salinity gradients. Münchow *et al.* (1992a) and Münchow and Garvine (1992) show that the subtidal flow in this source region of the coastal current always turns anti-cyclonically to form the Delaware

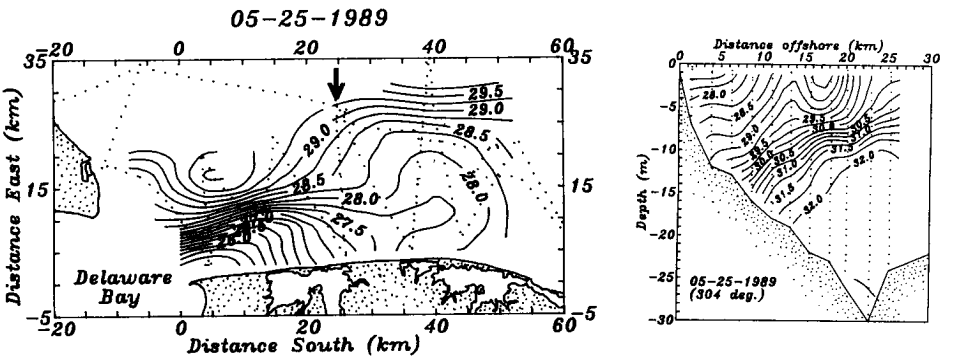

Figure 6. Map of surface salinity for the coastal current in May 1989 after a large river discharge event. Dots indicate the ship track along which we collected the data while the arrow indicates the location of a salinity transect shown to the right. For currents, winds, and discharge conditions during the event see Figure 3.

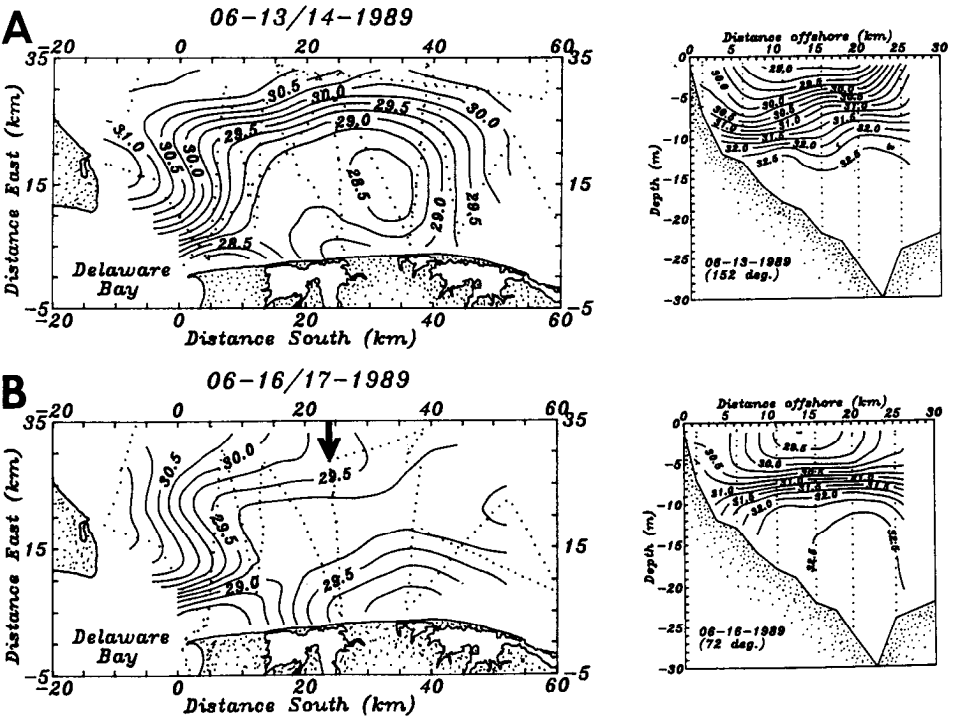

Figure 7. As Figure 6 but during strong upwelling favorable winds on (a) June 13/14, and (b) June 16/17 of 1989.

Coastal Current. On the shelf farther downstream buoyant waters widen and the lateral salinity gradients weaken. From the CTD transect across the buoyant plume we infer that buoyant waters contact the bottom. Wong and Münchow (1992) and Münchow and Garvine (1992) argue that this feature distinguishes the Delaware Coastal Current from many other buoyancy driven flows. Strong upwelling favorable winds and weaker buoyancy forcing, however, can change both the vertical and the horizontal distribution of estuarine water on the shelf. We present a vivid example next.

Three weeks after we completed the mapping of Figure 6 we profiled the inner shelf again. We obtained hydrographic and flow field information during a strong upwelling favorable event. The ADCP measured currents from 5 m below the surface downward. We thus obtained no direct current information from the top 25% of the water column. Two successive salinity maps (Fig. 7), however, suggest advective processes near the surface. The first map near the onset of the upwelling favorable winds (Fig. 7a) shows an almost rectangular plume with across- and along-shelf dimensions of about 30 km and 40 km, respectively. From the vertical salinity distribution of transect C (Fig. 8a) we see that isohalines still extend from the bottom to the surface, but are beginning to detach from the bottom. Three days later

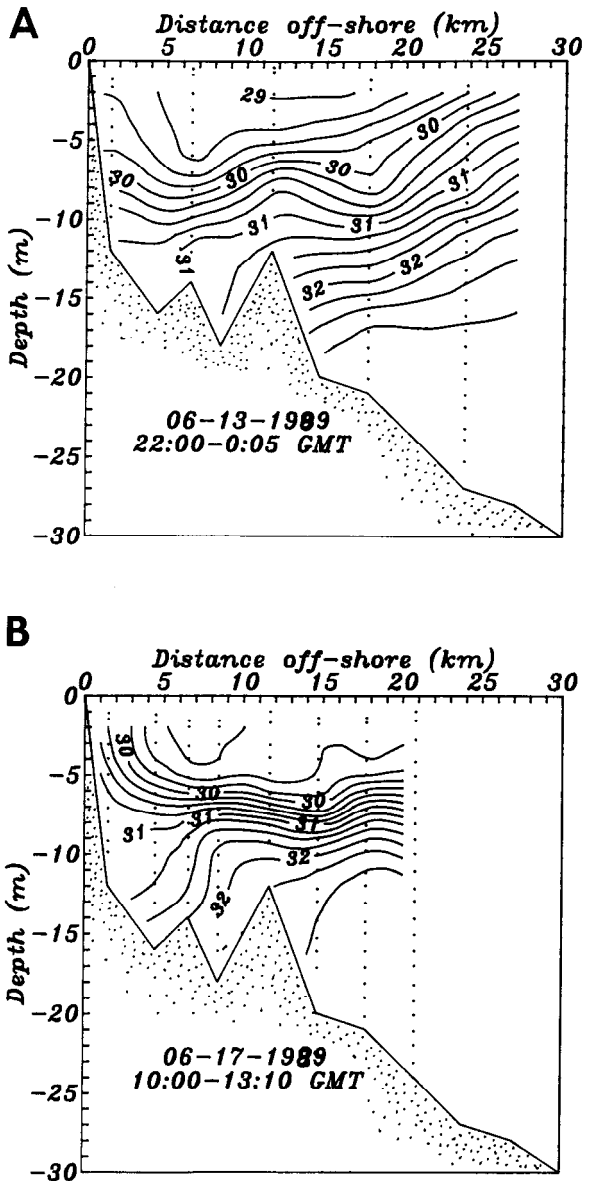

Figure 8. Salinity distribution on transect C. Data are from (a) near the onset (day 163, June 13, 1989) of upwelling favorable winds and (b) near their conclusion (day 168, June 17, 1989).

(Figs. 7b and 8b) buoyant waters occupy a surface layer only about 6 m deep. This layer now fills the entire study area across-shelf except near the coast where we now, instead, observe the highest salinities. Comparing the two maps, we conclude that the near shore buoyant waters move offshore. Inshore they are then replaced by

heavier waters from either downstream or the bottom. We exclude an upstream source of salty water as there the anti-cyclonically turning buoyant outflow always dominates the circulation (Fig. 7). The second salinity transect (Fig. 8b) shows that deeper, ambient shelf waters ($S > 32$ psu) do not reach the coast but apparently mix with the buoyant waters. We now find the strongest slopes of isolines within 8 km of the coast. Note, however, that strongly sloping isohalines inshore occur both near the surface and near the bottom. Isohalines near the surface slope in the classical upwelling sense with lighter water off-shore. At depth, in contrast, isohaline slopes indicate lighter waters inshore, i.e., a geostrophically balanced jet at depth opposes the local winds. Indeed we now observe the strongest subtidal downstream currents at depth (Fig. 9b).

For comparison we show in Figure 9 subtidal current vectors from upstream of the Delaware Estuary 46 hrs later. Off New Jersey buoyancy forcing is weak. The difference in the flows upstream of the estuary (off New Jersey) and downstream (off Delaware) is striking. Despite the winds being similar, currents near the surface upstream and downstream of the estuary move in opposite directions. In the absence of buoyancy forcing (off New Jersey) the flow 5 m below the surface is along-shore in the direction of the wind. Speeds reach 20 cm/s. In the presence of buoyancy forcing (off Delaware) the flow at the same depth is along-shore also, but opposes the wind. Speeds are about 5 cm/s. The flow 9 m below the surface differs as well. Upstream the current vector rotates counter clockwise with depth and the flow at 9 m is onshore. Downstream no rotation of current vectors with depth is apparent, but the along-shore current against the wind strengthens with depth.

In summary, strong upwelling favorable winds affect the buoyancy driven flow on the inner shelf. The wind spreads buoyant waters over ambient shelf waters offshore, while it forces dense ambient shelf waters underneath the buoyant waters toward the coast. This induced across-shelf circulation enhances vertical stratification. As a result, the buoyancy driven flow then no longer "feels" the bottom. While all the above observations are qualitatively consistent with linear Ekman dynamics, they also imply the nonlinear advection of buoyancy. Next, however, we discuss the interaction of wind driven and buoyancy driven motion more generally using observations from drogued drifters.

c. Drifter observations. The ARGOS satellite system provides between 6 and 8 positions per day for each drifter with an accuracy of better than 350 m. To each trajectory we fit a cubic spline and subsample position data every 3 hours. Finally we separate the data from different deployments by the respective wind direction during their deployment periods. In Figures 10a, 10b, and 10c we depict drifter trajectories during downwelling, upwelling, and transitional winds, respectively. Common to all experiments is the downstream displacement. About 20 km from the coast, however, the offshore velocity component becomes dominant while inshore surface currents frequently oppose the local winds due to the strong buoyancy forcing. When winds

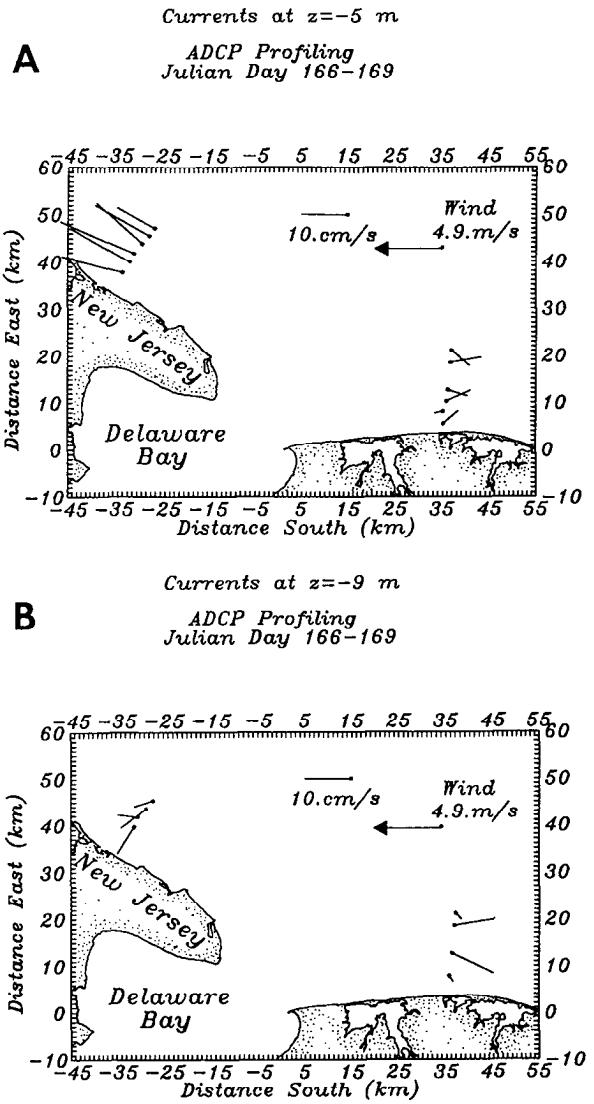

Figure 9. Maps of ADCP current vectors. Subtidal currents in June 1989 are from 5 m and 9 m below the surface and are not synoptic. Transects were profiled in sequence C and A on day 168 (June 17), and 169 (June 18). The wind vector shown is from a 3 day low-pass filtered series hence does not represent daily fluctuations. Off New Jersey note the turning of current vectors toward the coast near the bottom. The subtidal wind vector is shown at the upper right of each map. Off Delaware currents oppose the local wind.

are downwelling favorable (Fig. 10a) the downstream displacement is swift, since then wind and buoyancy act in concert.

We observe much smaller displacements and speeds during upwelling favorable winds (Fig. 10b), but inshore currents are still downstream with an offshore velocity

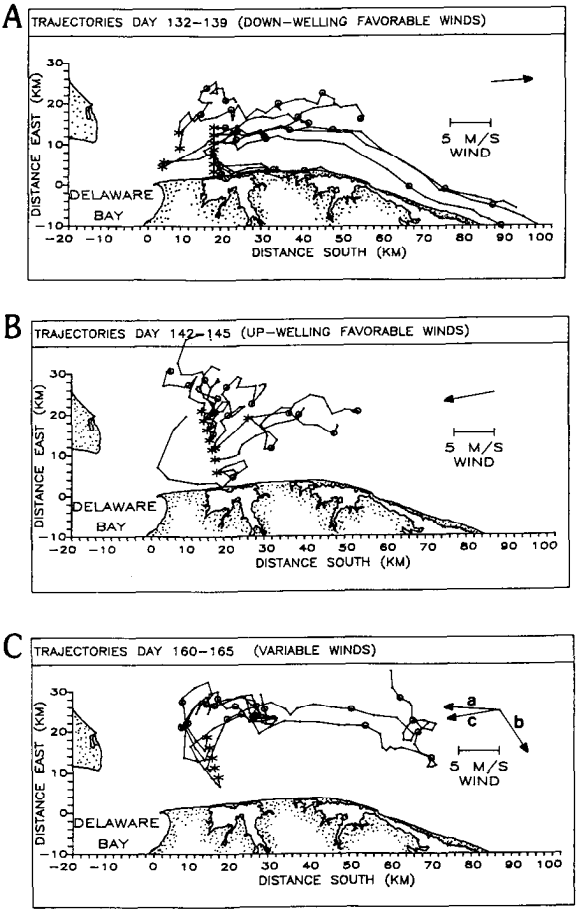

Figure 10. Drifter trajectories sorted by wind direction. (a) downwelling favorable winds; (b) upwelling favorable winds; (c) transitional winds. The wind vector and scale appears on the right of each figure. We added open circles every 24 hour after each drifter's deployment. We mark the deployment locations by a star.

component that increases in the offshore direction. The resulting divergence must be compensated by upwelling. Qualitatively, this is consistent with an "Ekman" layer response to winds superposed on a downstream buoyancy driven coastal current. We suspect, however, that surface and bottom Ekman layers overlap in water only 15 to 20 m deep. We tested this hypothesis by fitting Ekman's (1905) solutions to detided vertical ADCP current profiles that we measured on day 169 on transect A (see Fig. 9). The Ekman number $E = (\delta/D)^2$ is the only free parameter in the fit (not shown) and represents the ratio between the Ekman layer depth $\delta = (2A/f)^{1/2}$ and the water depth D. Here A and f are the vertical eddy viscosity and the Coriolis parameter, respectively. We find the best agreement between model and data for

Ekman numbers between 0.4 and 0.8, i.e., the Ekman layer is about 11 m deep or the eddy viscosity is about 50 cm^2/s. Ekman (1905) then predicts a surface current direction of less than 10 degrees clockwise from the wind direction for waters that are only 15 m deep. Csanady (1978) predicts a vertically averaged flow in the direction of the wind as he postulates a balance between surface and bottom stresses in the coastal boundary layer. Neither is the case in Figure 10b. Instead, we interpret the trajectories as a linear superposition of buoyancy and wind forced motion. Within the coastal current buoyancy dominates over wind forcing, while offshore the reverse holds.

Finally, in Figure 10c we show trajectories from a deployment 4 days long. Winds change rapidly from one day to the next from upwelling favorable to downwelling favorable and back. This experiment thus combines effects of Figures 10a and 10b. Initially drifters move offshore, again at an angle about 60 degrees to the right from the wind, before turning anti-cyclonically and swiftly racing downstream. Finally, the drifters again adjust to the new upwelling favorable winds by moving offshore. Note that the response to the wind is rapid, about 6 hours.

4. Statistics

Long time series of velocity data from moored current meters allow us to analyze the temporal variability of currents on the shelf. In the time domain we compute cross-correlations with winds and freshwater discharge rates, while in the frequency domain we estimate the coherence of currents at different locations. Drifter data, in contrast, allow us to analyze the spatial variability of the flow and the mixing that fluctuating motion causes. The analysis will reveal that wind and buoyancy forcing dominate processes at different time scales and locations.

a. Time domain. From 5 current meters moored 6 m and 10 m below the surface off Delaware (see Fig. 1 for locations) we compute lagged cross-correlations between along-shore winds (rotated to 190°T) and along-shore currents (rotated into the local downstream major principal axis). Positive lags imply currents that lag the winds. The results (Fig. 11a) mirror those of previous studies on inner shelves (Csanady, 1978; Pettigrew, 1981; Hopkins and Swoboda, 1986). Peak correlations of about 0.6 ± 0.15 occur at a lag of only 6 hrs. The 15% uncertainty represents a standard error (Bartlett, 1978) that assumes zero true correlation between the two variables. The degrees of freedom we obtain by dividing the record length by the decorrelation time scale. The latter we estimate from the integral of the auto-correlation function to its first zero crossing. In Figure 11 we use shading to show correlations that differ significantly from zero. We do not find significant differences in cross-correlations between currents at 6 m and at 10 m below the surface and thus suggest that the response is barotropic.

The response of the across-shelf flow component to the same along-shore wind is

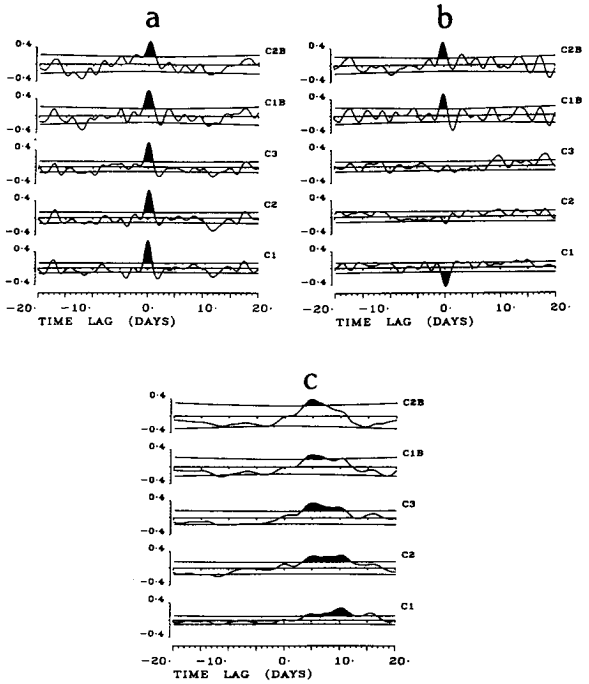

Figure 11. Lagged cross-correlations. (a) Along-shore winds and along-shore currents; (b) along-shore winds and across-shore currents; (c) freshwater discharge and along-shore currents. Correlations that are significant at the 95% confidence level are shown with shading. C1B and C2B refer to data from near the bottom at locations C1 and C2, respectively. See Figure 3 for mooring locations.

shown in Figure 11b. Maximum correlation still occurs at about 6 hour lag. The correlations 6 m below the surface are barely significant and negative, i.e., downwelling favorable winds correlate with onshore flows. In contrast, the correlations 10 m below the surface (about 7 m above the bottom) are much stronger (0.5 ± 0.15) and positive, i.e., downwelling favorable winds correlate with an offshore flow. The somewhat weaker correlation 6 m below the surface we explain with stronger buoyancy forcing there.

The final cross-correlation that we present is between the along-shore current and the freshwater discharge rates of the Delaware River, the principal source of buoyancy flux. Correlations are weaker than they were for the wind (0.3 ± 0.15) and maximum lag occurs between 5 and 10 days (Fig. 11c). Hence it takes almost 10 days for the discharge to reach the shelf. In Figure 11c we note that the lag time of currents close to the shore at C1 exceeds the lag time at C3 which is located 15 km from the coast. Currents at C3 thus respond to changes in freshwater discharge first and strongest. The latter we demonstrate next with a linear multiple regression

Table 2. Time domain multiple regression.

Station (distance offshore, km)	Along-shelf dir. (°T)	Mean speed (cm/s)	a $\left(\frac{\text{cm/s}}{\text{m/s}}\right)$	b $\left(\frac{\text{cm/s}}{10^3\text{m}^3/\text{s}}\right)$	Time lag τ_1, τ_2 (hrs)
C1 (4.5)	195	4.0	1.17 ± 0.31	4.7 ± 3.1	6,240
C2 (8.4)	200	3.3	1.63 ± 0.40	6.0 ± 4.1	6,240
C3 (14.7)	181	6.5	1.26 ± 0.39	7.7 ± 4.0	6,120

analysis between currents, winds, and freshwater discharge from the Delaware River.

From time series of along-shelf currents, local along-shelf winds, and freshwater discharge rates we first subtract the respective temporal mean and subject the data to the model

$$U(t) = \overline{U} + a\,[W(t - \tau_1) - \overline{W}] + b\,[R(t - \tau_2) - \overline{R}]$$

where U, W, and R represent the current, wind, and river discharge values at times t, $t - \tau_1$, and $t - \tau_2$, respectively, and overbars denote the record mean values. The regression coefficients a and b are determined by a least squares error criterion. They measure how effective the wind and discharge rates are in generating a current response. We choose the lag times τ_1 and τ_2 to be 6 hours and 5–10 days, respectively. Table 2 lists our choices along with the regression coefficients and the 95% confidence limit of these coefficients. We do not repeat details of the error estimation in multiple regression analysis, as we followed closely the concise discussion of Fofonoff and Bryden (1975).

The respective size of the regression coefficients a and b compare the respective magnitude of current fluctuations due to fluctuations in the local winds and the buoyancy forcing. About 15 km from the coast at mooring C3, for example, increasing the discharge rate by 500 m^3/s causes the downstream current to increase by about 4 cm/s, while more inshore at C1 the same discharge increases the current by only 2 cm/s. To offset this 4 and 2 cm/s increase of the current one needs an increase of upwelling favorable wind of about 3 and 2 m/s for C3 and C1, respectively. The mean current, however, in the presence of the mean wind (−1.5 m/s, i.e., upwelling favorable) and the mean discharge rate (525 m^3/s) is in the downstream direction also (7 cm/s at C3 and 4 cm/s at C1). Hence, only upwelling favorable wind speeds that exceed about 7 m/s can reverse the downstream currents at C3 during mean discharge rates. Such strong and upwelling favorable wind events, however, are rare during the spring and summer in the Mid Atlantic Bight. We then conclude that the downstream current is common for the Delaware Coastal Current during the spring and summer.

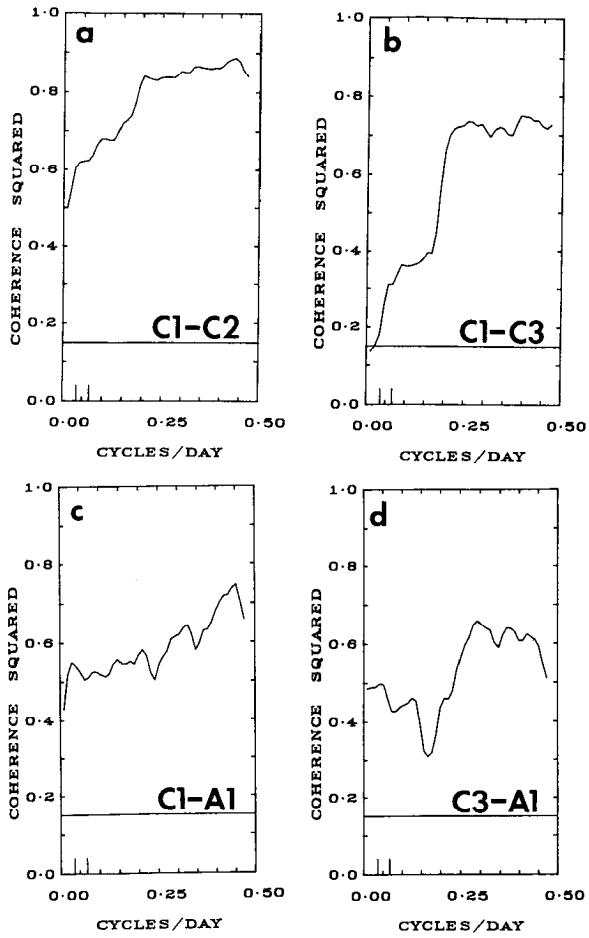

Figure 12. Coherencies of along-shore surface currents. The spatial separations are (a) 3 km across-shore off Delaware; (b) 10 km across-shore off Delaware; (c) 70 km along-shore; (d) 75 km along-shore.

b. Frequency domain. We now assume a linear input/output relation in the frequency domain between surface currents at various locations. The input time series in Figures 12a, b, and c is the along-shore velocity component at C1. The output time series are the along-shore velocity components from moorings that are located 70 km upstream (A1) of C1, 3 km offshore (C2) of C1, and 10 km offshore (C3) of C1. For comparison we also compute the coherence between currents at C3 and A1 (Fig. 12d), the two locations where we often find the largest currents. We smoothed spectral properties with a window 20 frequency intervals wide, resulting in 40 degrees of freedom, and hence obtained a 95% confidence level of 0.17.

Figure 12a shows the coherence of current between C1 and C2. The station separation is only about 3 km and consequently 90% ($\Gamma^2 \approx 0.9$) of the surface

current variance at C1 correlates with that at C2 at high frequencies (>0.25 cpd). At low frequencies (<0.1 cpd), however, the coherence drops to about 0.5. The phase (not shown) indicates that currents at C1 lead those at C2 with a constant time delay of only a few hours. The coherence between currents at C1 and C3 exhibits contrasting behavior at low frequencies (Fig. 12b). At 0.05 cpd only 20% of the variance inshore (C1) correlates with that 10 km farther offshore (C3). The phase (not shown) indicates little difference. Finally, we correlate currents off Delaware with those 70 km upstream off New Jersey (Figs. 12c and 12d). In contrast with coherencies across the shelf off Delaware, we find lower coherencies at high frequencies ($\Gamma^2 \approx 0.6$), but coherencies at low frequencies that always exceed 0.4. All results are significant at the 95% confidence level. In summary we conclude that currents in the coastal current off Delaware at periods larger than 10 days are more coherent 70 km along the shelf than 10 km across it.

What is the cause for the very different coherencies along and across the shelf? We argue that in different parts of frequency space different processes contribute differently to the current variance at different locations. The wind dominates on the ambient shelf, such as off New Jersey, at all frequencies. In the coastal current off Delaware, however, winds dominate at high frequencies (>0.2 cpd) only, while buoyancy forcing becomes sizable at low frequencies (<0.1 cpd). Further, we argue that while the buoyancy forced motion varies spatially in the across-shore direction (Table 2), the wind forced motion is spatially almost uniform, even for our along-shore scales. Applying these hypotheses to Figure 12 we explain the observed variability. Within 5 km of the coast at C1 and A1 buoyancy forcing is very weak, thus currents correlate well along the shelf at all frequencies. Comparing currents 5 km from the shore with those 15 km from it, in contrast, we find high correlations at high frequencies because the winds are spatially uniform and dominate the forcing. At low frequencies, in contrast, we find low correlations because the buoyancy forcing is stronger 15 km from the shore than it is 5 km farther inshore.

Finally, we present the results from a linear system analysis with two inputs (local wind and discharge) and a single output (current). We compute both the multiple coherencies, i.e., the overall current variance explained by both the wind and the discharge, and the partial or conditional coherencies. The latter measure the amount of current variance that is explained by one input after the coherent part between the two inputs, and thus its influence upon the output, has been removed (Bendat and Piersol, 1980). Figure 13 depicts all these coherencies for the surface currents at C3. At frequencies below 0.1 cpd only 40% of the current variance is explained by the linear system. Both the partial coherencies of the wind and the discharge are just barely above the 95% significance level. They are similar in magnitude and explain between 20% and 30% of the current variance. At higher frequencies, however, the linear system explains up to 70% of the current variance, but that is due to the wind alone. Our statistical results are marginally significant at best for the low frequencies.

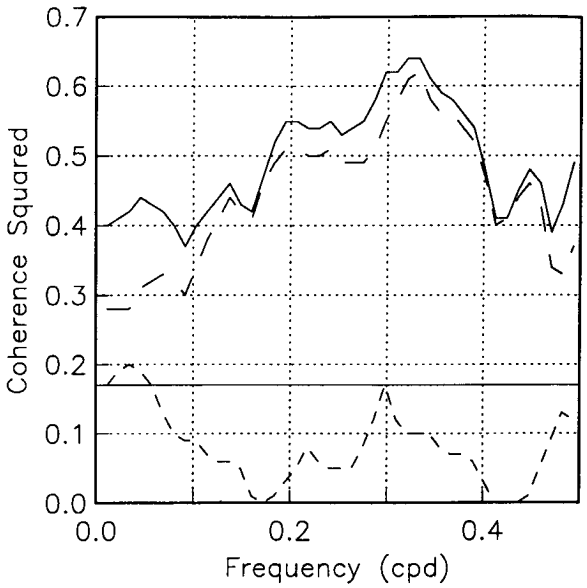

Figure 13. Multiple coherence between currents with the wind and freshwater discharge rates at C3 (solid line) and partial coherence between currents and freshwater discharge rates (short dash) and currents and winds (long dash). Note that at frequencies below 0.1 cpd wind and discharge each explain about 30% and 20% of the current variance, respectively.

In summary, we conclude that at high frequencies local wind forcing accounts for most of the current variance. At low frequencies, however, local wind and river discharge forcing combined explain less than half of the total variance, each making roughly equal contributions. About 60% of the variance at low frequencies is thus noise or related to other forcing processes. One other likely forcing agent is freely propagating coastally trapped vorticity waves. Noble *et al.* (1983) estimated that such waves in this region of the shelf contributed about 20% of the total subtidal current variance. Nevertheless, buoyancy forcing rivals wind forcing 15 km from the shore. In a geostrophic current that is in thermal wind balance we expect largest currents where lateral density gradients are largest. Largest density gradients we always observe seaward of our most off-shore mooring on transect C (see Figs. 6 and 7a). Additionally, lateral and vertical friction will retard currents close to the shore more than it will farther offshore. We thus conclude that the core of the buoyancy driven coastal current at transect C is located away from the coast.

c. Lagrangian perspective. In order to remove tidal and inertial variability from the drifter data, we subject the 3-hour subsampled position data (Fig. 10) to a fifth order polynomial which acts as a low-pass filter. Subtidal velocity estimates we then obtain by central differencing buoy positions at different times. We use Lagrangian auto-correlations to first estimate the degrees of freedom in the data set. The auto-

correlation $R(\tau)$ we define as

$$R(\tau) = \frac{\langle u'(t)\, u'(t+\tau)\rangle}{\langle u'^2(t)\rangle}$$

where

$$u(t) = \langle u\rangle + u'(t)$$

and

$$\langle u\rangle = \lim_{t\to\infty} \frac{1}{T}\int_0^T u(t)\, dt \approx \frac{1}{N}\sum_{i=1}^{N} u(t_i).$$

N represents the number of observations of an individual drifter and all properties are Lagrangian. Following Brink *et al.* (1991) and Poulain and Niiler (1989) we take the integral of $R(\tau)$ to the first zero crossing as an estimator of the decorrelation time scale T_D which then is about a day. This time scale is similar to those which we estimated for Eulerian current meter data (not shown).

In the following we present the spatial distribution of Eulerian mean currents and deviations thereof. In order to obtain statistically significant results we average all velocity data into spatial bins 10 and 20 km wide in the across- and along-shelf directions, respectively. We require the mean currents to have a preferred direction and thus apply the Raleigh test (Mardia, 1972) for non-uniform directional distribution of the data. Further, we require at least 8 degrees of freedom of any bin average. The latter condition assures that data from different deployments enters the average. We use only data passing both criteria in the subsequent analysis.

We summarize the results in Figure 14. All mean currents (Fig. 14a) are highly directional, as the 95% confidence levels for direction indicate. Mean currents beyond 20 km south are strong (>20 cm/s) and downstream. Also in Figure 14 we give the results from current meters moored 6 m below the surface and label them C1, C2, and C3. The mean currents from drifter and mooring data have different magnitudes and slightly different directions near the shore. Drifter speeds reach 20 cm/s while speeds from current meters never exceed 12 cm/s. Remember that the buoys are drogued 2 m below the surface, while the current meters are moored 6 m below the surface, and that the water is always shallower than 20 m. Forcing due to buoyancy increases from the bottom toward the surface where it is strongest and we expect currents 2 m below the surface to be stronger than those 20% farther down in the water column. Also, the centroid for each computed current vector from drifter data is closer to the source of the buoyancy and experiences stronger forcing. Farther offshore mean currents weaken as the result of smaller horizontal density gradients (see Figs. 6 and 7). We interpret Figure 14a as the Delaware Coastal Current in transition from anti-cyclonic turning to an along-shelf buoyancy driven coastal jet.

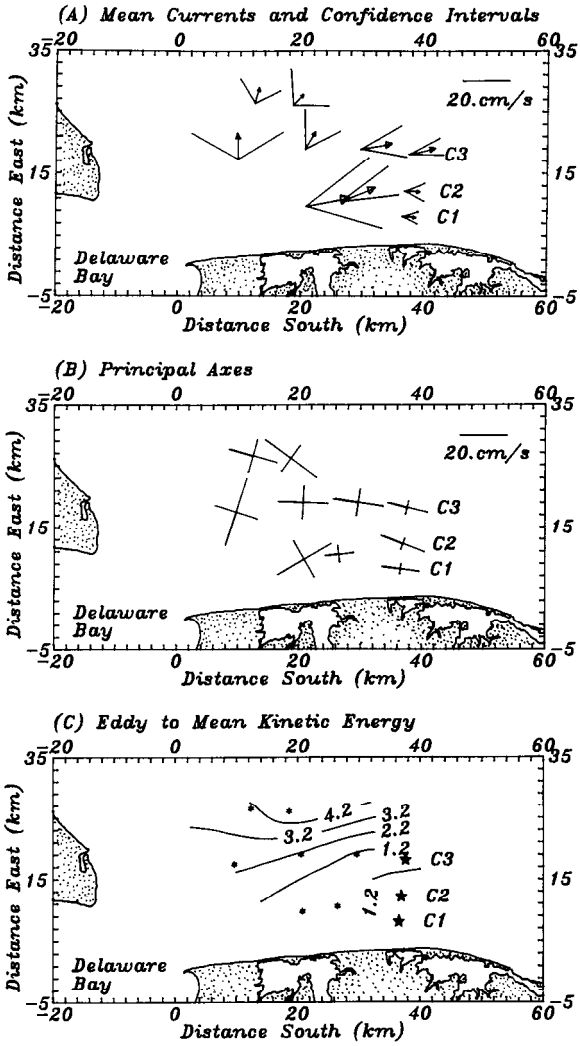

Figure 14. Eulerian statistics from drifter and current meter data. The latter data we label as C1, C2, and C3: (a) mean currents and 95% confidence intervals for speed and direction; (b) principal axes of the deviations from the mean; (c) ratio of eddy to mean kinetic energy.

Qualitatively similar transitions were found for buoyant outflows in the models of Chao and Boicourt (1986) and Garvine (1987).

The principal axes in Figure 14b represent the deviations from the mean currents of Figure 14a. The length of these axes are the square root of the eigenvalues of the Reynolds stress or covariance tensor (Freeland *et al.,* 1975; Kundu and Allen, 1976). Close to the estuary the major and minor axes are of similar magnitude, while farther downstream the deviations become more elliptical and the major axes are aligned

with the local topography. The magnitude of the major axes is about 10 cm/s and spatial variations are smaller and less organized than those of the mean currents. As a result, the ratio R_{em} of eddy (*eke*) to mean (*mke*) kinetic energy

$$R_{em} = \frac{eke}{mke} = \frac{\langle u'^2 + v'^2 \rangle}{\langle \bar{u}^2 + \bar{v}^2 \rangle}$$

is generally smaller than 5. Figure 14c shows this ratio and one might select the $R_{em} = 2$ contour as the offshore boundary of the coastal current. Farther offshore mean currents are weak, but the fluctuating currents are fairly uniform throughout the domain; hence R_{em} increases offshore. The core of the coastal current we identify as $R_{em} < 1.2$, which includes the mooring location C3.

Finally, we add a cautionary note and a physical interpretation of the results of this sub-section. The time scale for the "mean" currents of Figure 14a is only somewhat larger than a month. The "mean" thus represents subtidal variability at periods comparable to those of the buoyancy forcing. One can then view the "mean" as a snapshot of monthly variability. The fluctuations, on the other side, represent subtidal processes at higher frequencies which the wind dominates. Therefore, our discussion of mean vs. eddy motion (Fig. 14c) is more accurately one of subtidal variability at different frequencies.

d. Dispersion. While the last section presented Eulerian flow fields from drifter data, we now concentrate on the mixing which the fluctuating motion causes. Hence, we now view the drifters as quasi-Lagrangian particles and will describe how they disperse. In order to perform such an analysis one must assume that the turbulence of the flow is stationary and homogeneous. Stationarity of the flow field is essential, since only then can we replace ensemble averages by time averages (Chatwin and Allen, 1985). With homogeneous turbulence we mean that the velocity field is locally homogeneous, i.e., the mean horizontal velocity shear is constant (Monin and Yaglom, 1975) as it is in our application (Münchow and Garvine, 1992). Freeland *et al.* (1975) for example found that drifters from the Mid-Ocean-Dynamics-Experiment (MODE) described an inhomogeneous eddy field. Thus they could not rationally apply the theory of Taylor (1921) to describe the mixing of drifting particles. Colin de Verdiere (1983) and Krauss and Böning (1987) released drifters in the North-Atlantic and found that Taylor's theory described their dispersion well. They then computed dispersion coefficients which quantify the mixing the eddy field causes. Davis (1985) and Garrett *et al.* (1985) estimated mixing coefficients for the coastal ocean off California and Labrador, respectively. In the following we will closely follow the analysis of those authors and refer the reader to them for a discussion of the method. We will conclude with dispersion coefficients for the coastal current.

The dispersion of drifters will resemble a random walk for a time t long after

the deployment. "Long" means here long relative to the integral time scale $T_L = \int_0^\infty R(\tau)d\tau$, i.e., for $t \gg T_L$. In analogy with Fickian diffusion one defines a constant dispersion coefficient K as

$$K = \frac{1}{2}\frac{d\langle x'^2\rangle}{dt} = \langle u'^2\rangle T_L$$

where $\langle u'^2\rangle$ and $\langle x'^2\rangle$ are the mean square variance of a drifter velocity and its displacement, respectively. Both quantities are averaged over a Lagrangian ensemble. The mean has been removed from both the displacement and the velocity. In Figure 15a we present the time evolution of the variance or dispersion for the along- and the across-shore component of the displacement. After about 25 hours the dispersion indeed varies linearly with time, and the slope then determines K to be 1800 and 230 m^2/s in the along- and across-shelf direction, respectively. The reliability of these values depends crucially upon the mean having been removed accurately from the velocity data. One way to test this requirement is to compare the translation of the "center of gravity" $\langle x\rangle$ of the entire cloud of particles with the translation due to the ensemble and time averaged current $\overline{\langle u\rangle}t$. The overbar indicates the time average. Both translations we compare in Figure 15b and 15c. Indeed, for about 45 hours the mean cluster location moves with the mean current. We thus feel confident that the results up to that time are statistically robust, while those beyond are not. The number of degrees of freedom for $t < 45$ hours is larger than 50.

Since we now know the dispersion coefficient K we can estimate T_L from

$$T_L = \frac{K}{\langle u'^2\rangle} = (24,3) \text{ hours}$$

for the along- and across-shelf directions. While the very short across-shore time scale is probably a result of the poor estimation of the across-shelf dispersion coefficient, the Lagrangian integral time scale along the shelf agrees well with the Eulerian time scale. Following Davis (1985) we can then conclude that the flow field is linear, since Eulerian and Lagrangian integral time scales are similar.

5. Discussion

Local winds and lateral buoyancy fluxes from major estuaries constitute two major forcing mechanisms on many inner continental shelves. Here we reported observations from the inner shelf of the Mid Atlantic Bight where the water depth is less than 30 m. We find that the discharge of between 500 and 2000 m^3/s of freshwater from the Delaware River forces an along-shelf flow of about 20 cm/s in the direction of Kelvin wave phase propagation. This current frequently opposes the moderate but upwelling favorable winds. Velocity fluctuations, however, correlate well with the

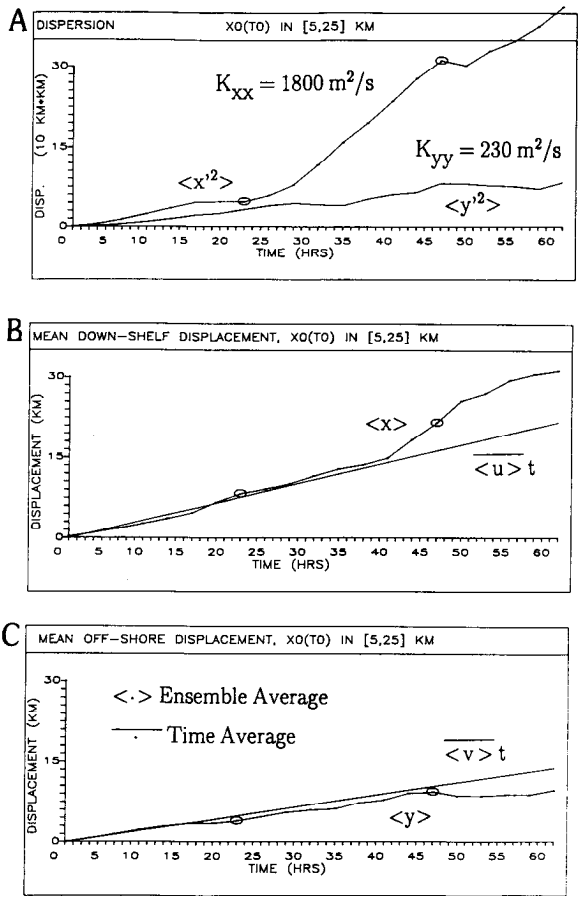

Figure 15. Results of drifter dispersion. (a) Drifter dispersion as a function of time after deployment and the derived dispersion coefficient in the along-shore (K_{xx}) and across-shore (K_{yy}) directions, respectively; (b) mean along-shelf displacements of drifter ensembles with time after deployment; the straight line is the displacement due to the time and ensemble averaged speed; (c) as (b) but for the across-shore displacements. The statistics are robust for about the first 40 hours.

local winds in the Ekman sense, i.e., during upwelling favorable winds the surface and bottom flows have a strong offshore and onshore component, respectively.

At the mouth of the Delaware Estuary the fresh water discharge represents a seaward buoyancy flux of about 80 m^4/s^3 at subtidal time scales. This horizontal buoyancy flux causes a pressure gradient on the inner continental shelf that is partly balanced by the Coriolis force of an along-shelf flow. Both drifter and moored current meter observations confirm this buoyancy driven coastal current that extends about 20 km across and more than 80 km along the shelf. The current varies between daily and monthly time scales. Generally upwelling favorable winds perturb but

seldom reverse the flow at daily scales. The same winds cause, however, mixing of buoyant coastal current and ambient shelf waters as they induce vertically sheared across-shelf flow components. We believe that our dispersion coefficients of about 2000 and 200 m^2/s in the along- and across-shelf direction, respectively, reflect short period wind forced motions that disperse fluid particles into and out of the coastal current.

The coastal current generally contacts the bottom as isohalines intersect both the surface and the bottom. Only during exceptionally strong upwelling favorable winds does the buoyant outflow form a shallow plume that constitutes a distinct surface layer. The plume waters then spread across the shelf and, presumably, are mixed away by the different flow regimes of the middle and outer shelf. From a multiple regression analysis in the time domain more quantitative results emerged. In order to arrest the buoyancy driven coastal current, upwelling favorable winds have to exceed about 7 m/s for mean river discharge conditions. High discharge rates and moderate winds during the spring and summer thus rarely allow the downstream current to reverse. This important result clashes with predictions of a numerical model of our study area. We next briefly discuss the model and then contrast its results with our observations.

The three dimensional finite difference model of Galperin and Mellor (1990) seeks to model all aspects of estuarine shelf interaction of the Delaware River, the Delaware Estuary, and the adjacent continental shelf. The model utilizes sophisticated turbulence closure, realistic topography, and prescribes tidal, wind, freshwater discharge, and surface heat flux forcing functions from observations along boundaries. The resolution is 1 km and 4 km within the estuary and on the shelf, respectively. A matching condition is applied at the mouth of the estuary.

Galperin and Mellor (1990) use data from current meter moorings and tide gauges inside the estuary for most of 1984 to both initialize and calibrate their model. Moses-Hall (1992) analyzed this data set and reports an annual mean discharge rate of 490 m^3/s with peak discharge in March and June exceeding 3000 m^3/s. These values are similar to those for 1989. Local winds in 1984 were also similar to those of 1989, moderate and generally upwelling favorable in spring and summer. We thus expect that both the flow and the salinity fields on the shelf should be similar in both years, also. Indeed, during the near absence of wind forcing in April 1984 Galperin and Mellor (1990) predict a brackish plume on the shelf that turns anti-cyclonically and is little affected by tidal currents consistent with our observations. The model fails, however, to reproduce a coastal current downstream of the mouth of the estuary in the presence of either upwelling or downwelling favorable winds at either the monthly or the several day time scale.

The model responded to an upwelling favorable (northward) wind stress of 0.072 N/m^2, corresponding to a wind speed of about 5 m/s on July 2, 1984 with a flow in the direction of the wind (Galperin and Mellor, 1990). Discharge rates prior to the

event were about 500 m^3/s. In the model such wind and discharge conditions forced the buoyant estuarine waters to exit the estuary cyclonically. The model thus predicted brackish waters that moved upstream. We, in contrast, never observed such a cyclonic turning of the coastal current. Instead, during very similar river discharge and wind conditions in June 1989 we found a seaward flowing, anti-cyclonically turning, 10 cm/s strong coastal current at the mouth of the estuary. According to our hindcasting model, the July 1984 wind and discharge values were insufficient to even reverse the coastal current 40 km downstream from the mouth of the estuary. Hence, the likelihood that a moderate wind speed of 5 m/s can reverse the currents at the mouth of the estuary is low.

From our time series of wind and current vectors (Fig. 3) we infer that currents at C3 reversed only once, near day 150 when the local winds were northward and exceeded 8 m/s. Nevertheless, profiling the shelf two weeks later (Fig. 7a) we found a well developed coastal current despite moderately upwelling favorable winds at a discharge rate below the annual mean. In contrast, during downwelling favorable winds 20 days after a strong upwelling event the model results (Galperin and Mellor, 1990, Fig. 15, p. 273) neither indicate a coastal current nor brackish waters downstream, even though the fresh water discharge rates then are above the annual mean. The model thus seems too sensitive to wind forcing while insufficiently sensitive to buoyancy forcing. It thus fails to reproduce the results of the joint forcing of wind and buoyancy that we observed.

Our linear hindcast model accounts for less than 50% of the current variance at time scales longer than 10 days. We thus do not claim to fully understand all aspects of the dynamics. Nonlinear processes, instabilities of the coastal current, and free coastally trapped vorticity waves all may contribute to the low coherence between currents and local winds and between currents and discharge rates. The interaction of the buoyancy driven coastal current with bottom stresses is still unclear. The detailed dynamics of the region of large lateral density gradients off-shore requires special attention. This study, however, does not allow us to properly quantify frontal structures and their response to variable wind and buoyancy forcing. Finally, close to the shore in water less than 10 m deep, swell and breaking waves may well affect the local circulation there.

Nevertheless, our observations revealed at least qualitatively how buoyancy and wind forcing interact in the Delaware Coastal Current, a buoyancy driven coastal current on the inner continental shelf. Only strong upwelling favorable winds reverse the buoyancy driven flow on the shelf. These events, however, are rare during spring and summer, and the winds thus mainly constitute a mixing agent for the buoyant discharge. In the Mid Atlantic Bight estuarine material is thus mainly advected downstream along the coast during the spring and summer.

Acknowledgments. The competent and good humored crew of the R/V *Cape Henlopen* under their captain, Donald McCann, enabled us to collect the data set in a most enjoyable fashion.

The technical assistance at sea of Timothy Pfeiffer was crucial to analyze the ship-board data near real time. At sea many friends shared hands and brains. Arthur Sundberg competently designed and constructed the drifters for this study. Robert McCarthy recovered and redeployed the drifters repeatedly and helped with many fruitful discussions. Two anonymous reviewers provided detailed and constructive criticism. The National Science Foundation of the U.S.A. funded this study through grant OCE-8816009.

REFERENCES

Allen, J. S., R. C. Beardsley, J. O. Blanton, W. C. Boicourt, B. Butman, L. C. Coachman, A. Huyer, T. H. Kinder, T. C. Royer, J. D. Schumacher, R. L. Smith, W. Sturges, C. D. Winant. 1983. Physical oceanography of continental shelves. Rev. Geophys. Space Phys., *211,* 1149–1181.

Bartlett, M. S. 1978. Stochastic Processes. 3rd ed., Cambridge University Press, New York, NY, 287 pp.

Beardsley, R. C., R. Limeburner, H. Yu and G. A. Cannon. 1985. Discharge of the Changjiang (Yantze River) into the East China Sea. Cont. Shelf Res., *4,* 57–76.

Bendat, J. S. and A. G. Piersol. 1978. Engineering Applications of Correlation and Spectral Analysis. John Wiley, New York, NY, 302 pp.

Blanton, J. O. 1981. Ocean currents along a nearshore frontal zone on the continental shelf of the eastern United States. J. Phys. Oceanogr., *11,* 1627–1637.

Bowman, M. J. and R. L. Iverson. 1978. Estuarine and plume fronts, *in* Oceanic fronts in coastal processes, M. Bowman and W. E. Esaias, eds. Springer Verlag, New York, NY, 114 pp.

Brink, K. H. 1991. Coastally-trapped waves and wind-driven currents over the continental shelf. Ann. Rev. Fluid Mech., *23,* 389–412.

Brink, K. H., R. C. Beardsley, P. P. Niiler, M. Abbott, A. Huyer, S. Ramp, T. Stanton and D. Stuart. 1991. Statistical properties of near-surface flow in the California Coastal Transition Zone. J. Geophys. Res., *96,* 14693–14706.

Chao, S.-Y. and W. C. Boicourt. 1986. Onset of estuarine plumes. J. Phys. Oceanogr., *16,* 2137–2149.

Chatwin, P. C. and C. M. Allen. 1985. Mathematical models of dispersion in rivers and estuaries. Ann. Rev. Fluid Mech., *17,* 119–149.

Colin de Verdiere, A. 1983. Lagrangian eddy statistics from surface drifters in the eastern North Atlantic. J. Mar. Res., *41,* 375–398.

Csanady, G. T. 1978. The arrested topographic wave. J. Phys. Oceanogr., *8,* 47–62.

Davis, R. E. 1985. Drifter observation of coastal surface currents during CODE: The statistical and dynamical views. J. Geophys. Res., *90,* 4756–4772.

Davis, R. E., J. E. Dufour, G. P. Parks and M. R. Perkins. 1982. Two inexpensive current-following drifters. Scripps Institution of Oceanography reference no. 82–28.

Ekman, V. W. 1905. On the influence of the earth's rotation on ocean currents. Ark. Mat. Astronom. Fys., *2,* 55–108.

Fofonoff, N. P. and H. L. Bryden. 1975. Density of seawater. J. Mar. Res., *41,* 69–82.

Freeland, H. J., P. B. Rhines and T. Rossby. 1975. Statistical observations of the trajectories of neutrally buoyant floats in the North Atlantic. J. Mar. Res., *33,* 383–404.

Galperin, B. and G. L. Mellor. 1990. A time dependent, three-dimensional model of the Delaware Bay and River system. Part II: Three-dimensional flow field and residual circulation. Estuar. Coast. Shelf Sci., *31,* 255–281.

Garrett, C., J. Middleton, M. Hazen and F. Majaess. 1985. Tidal currents and eddy statistics from iceberg trajectories off Labrador. Science, *227,* 1333–1335.

Garvine, R. W. 1991. Subtidal frequency estuary-shelf interaction: Observations near Delaware Bay. J. Geophys. Res., *96,* 7049–7064.

—— 1987. Estuary plumes and fronts in shelf waters: a layer model. J. Phys. Oceanogr., *17,* 1877–1896.

Giessen, A. van der, W. P. M. de Ruijter and J. C. Borst. 1990. Three dimensional current structure in the Dutch coastal zone. Neth. J. Sea Res., *25,* 45–55.

Griffiths, R. W. and A. F. Pearce. 1985. Instability and eddy pairs on the Leeuwin Current south of Australia. Deep Sea Res., *32,* 1511–1534.

Hopkins, T. S. and A. L. Swoboda. 1986. The nearshore circulation off Long Island, August 1978. Cont. Shelf Res., *5,* 431–473.

Houghton, R. W., R. Schlitz, R. C. Beardsley, B. Butman and J. L. Chamberlin. 1982. The Middle Atlantic Bight cold pool: Evolution of the temperature structure during summer 1979. J. Phys. Oceanogr., *12,* 1019–1029.

Johannessen, J. A., E. Svendsen, S. Sandven, O. M. Johannessen, and K. Lygre. 1989. Three dimensional structure of meso scale eddies in the Norwegian Coastal Current. J. Phys. Oceanogr., *19,* 3–19.

Krauss, W. and C. W. Böning. 1987. Lagrangian properties of eddy fields in the northern North Atlantic as deduced from satellite-tracked buoys. J. Mar. Res., *45,* 259–291.

Kundu, P. K. and J. S. Allen. 1976. Some three dimensional characteristics of low frequency current fluctuations near the Oregon coast. J. Phys. Oceanogr., *6,* 181–199.

Mardia, K. V. 1972. Statistics of Directional Data. Academic Press, San Diego, CA, 357 pp.

Masse, A. K. 1988. Estuary shelf interaction: Delaware Bay and the inner shelf. PhD thesis, University of Delaware, Newark, DE.

Mitchum, G. T. and A. J. Clarke. 1986. The frictional nearshore response to forcing by synoptic scale winds. J. Phys. Oceanogr., *16,* 934–946.

Monin, A. S. and A. M. Yaglom. 1975. Statistical Fluid Dynamics, Vol. 2, MIT Press, Cambridge, MA.

Moses-Hall, J. 1992. Observed tidal, subtidal, and mean properties in a laterally variable coastal plain estuary. PhD Dissertation, University of Delaware, Newark, DE, 337 pp.

Münchow, A. and R. W. Garvine. 1992. Dynamical properties of a buoyancy driven coastal current. J. Geophys. Res., (submitted).

Münchow, A., R. W. Garvine and T. F. Pfeiffer. 1992a. Subtidal currents from a shipboard acoustic doppler current profiler in tidally dominated waters. Cont. Shelf Res., *12,* 499–515.

Münchow, A., A. K. Masse and R. W. Garvine. 1992b. Astronomical and nonlinear tidal currents in a coupled estuary shelf system. Cont. Shelf Res., *12,* 471–498.

Noble, M., B. Butman and E. Williams. 1983. On the longshelf structure and dynamics of subtidal currents on the eastern United States continental shelf. J. Phys. Oceanogr., *13,* 2125–2147.

Pettigrew, N. R. 1981. The dynamics and kinematics of the coastal boundary layer off Long Island. PhD thesis, MIT/WHOI.

Poulain, P.-M. and P. P. Niiler. 1989. Statistical analysis of the surface circulation in the California Current system using satellite-tracked drifters. J. Phys. Oceanogr., *19,* 1588–1603.

Royer, T. C. 1983. Observations of the Alaskan Coastal Current, *in* Coastal Oceanography, H. Gade, A. Edwards and H. Svendsen eds., Plenum Publishing Corp.

Simpson, J. H. and A. E. Hill. 1986. The Scottish Coastal Current, *in* The role of freshwater outflow in coastal marine ecosystems, S. Skreslet, ed., NATO ASI Series G.: Ecological Science, Vol. 7, 453 pp.

Taylor, G. I. 1921. Diffusion by continuous movements. Proc. London Math. Soc., *A20,* 196–211.

Winant, C. D. 1980. Coastal circulation and wind induced currents. Ann. Rev. Fluid Mech., *12,* 271–301.

Wong, K.-C. and A. Münchow. 1992. Buoyancy forced interaction between estuary and inner shelf: observation. Cont. Shelf Res., (submitted).

Received: *6 October, 1992;* revised: *18 January, 1993.*